Published in final edited form as:
Neuroscience. 2008 June 12; 154(1): 283–293. doi:10.1016/j.neuroscience.2008.01.010.

Branched Projections in the Auditory Thalamocortical and Corticocortical Systems

Amar U. Kishan, **Charles C. Lee**, and **Jeffery A. Winer**
Division of Neurobiology, Department of Molecular and Cell Biology, University of California at Berkeley, Berkeley, CA 94720-3200, USA

Abstract

Branched axons (BAs) projecting to different areas of the brain can create multiple feature-specific maps or synchronize processing in remote targets. We examined the organization of BAs in the cat auditory forebrain using two sensitive retrograde tracers. In one set of experiments (n=4), the tracers were injected into different frequency-matched loci in the primary auditory area (AI) and the anterior auditory field (AAF). In the other set (n=4), we injected primary, non-primary, or limbic cortical areas.

After mapped injections, percentages of double labeled cells (PDLs) in the medial geniculate body (MGB) ranged from 1.4% (ventral division) to 2.8% (rostral pole). In both ipsilateral and contralateral areas AI and AAF, the average PDLs were <1%. In the unmapped cases, the MGB PDLs ranged from 0.6% (ventral division) after insular cortex injections to 6.7% (dorsal division) after temporal cortex injections. Cortical PDLs ranged from 0.1% (ipsilateral AI injections) to 3.7% AII (contralateral AII injections). PDLs within the smaller (minority) projection population were significantly higher than those in the overall population.

About 2% of auditory forebrain projection cells have BAs and such cells are organized differently than those in the subcortical auditory system, where BAs can be far more numerous. Forebrain branched projections follow different organizational rules than their unbranched counterparts. Finally, the relatively larger proportion of visual and somatic sensory forebrain BAs suggests modality specific rules for BA organization.

Keywords

axon collaterals; maps; axons; collateral projections; projections; double labeling

INTRODUCTION

Each of the thirteen areas of cat auditory cortex (AC) (Fig. 1A) receives robust afferent input from the medial geniculate body (MGB) and the ipsi- and contralateral AC (Winer and Lee, 2007). The degree to which thalamocortical and corticocortical neurons with branched axons (BAs) participate in these several projection systems is of interest since such cells could create independent computational processes at different target loci. The organization and number of axon collaterals within these systems is unknown and are the subjects of this report.

Correspondence to: Jeffery A. Winer, Department of Molecular and Cell Biology, Division of Neurobiology, Room 289 Life Sciences Addition, University of California at Berkeley, Berkeley, CA 94720-3200, Email: jaw@berkeley.edu, Telephone: (510) 642-8227, Fax: (510) 643-6791.

BAs can create feature-specific maps or synchronize processing within remote brain regions (Schofield et al., 2007). Although there are at least five maps of characteristic frequency (CF) within AC (Morel and Imig, 1987), there are only two within the MGB, one in the rostral pole (RP) and another in the ventral division (MGBv) (Aitkin and Webster, 1972; Imig and Morel, 1985). Thalamocortical (TC) BAs could account for the expansion of the two MGB tonotopic representations into the several AC maps: the axon of a cell responsive to a given CF may branch and terminate in more than one AC region representing that CF. Prior work testing this model reported data from a small sample of tissue (Morel and Imig, 1987) or was limited to only two areas (Lee et al., 2004a). Thus, the differential areal contribution of BAs in the AC commissural and ipsilateral corticocortical pathways remains unknown, though the proportion of double labeled cells after frequency-matched injections is <1.5% (Lee et al., 2004a).

To re-examine the organization of BAs systematically, we injected frequency-matched loci in the primary auditory cortex (AI) and the anterior auditory field (AAF) with two sensitive retrograde tracers, the β subunit of cholera toxin (CT β) (Luppi et al., 1990), and a gold-conjugated variant (CTβG) (Llewellyn-Smith et al., 1990), and analyzed the ensuing nuclear and areal distribution of double labeled neurons (DLs). Intraareal branching in each of the three major projection systems was examined for each functional class of AC areas by injecting CTβ and CTβG into primary, non-primary, multisensory, and limbic cortex. We occasionally substituted wheat-germ apo-horseradish peroxidase gold-conjugate (WAHG) (Basbaum and Menetrey, 1987; Winer et al., 1996), an equally sensitive tracer, for CTβG.

BAs are a small but common constituent of auditory forebrain projection systems, suggesting that they are not a likely source for creating and/or modulating the spectral maps in AI and AAF. The spatial distribution of the few BAs suggests that they follow different organizational parameters than unbranched axons. The few auditory forebrain BAs contrasts with their relative abundance in the subcortical auditory system (Irvine, 1986). Finally, the relatively larger percentage of BAs in the visual (Bullier, 1984; Bullier et al., 1984a; Birnbacher and Albus, 1987; Salin et al., 1989) and possibly somatic sensory (Spreafico et al., 1981; Fisher et al., 1983) forebrain suggests modality specific patterns for branched axonal organization.

EXPERIMENTAL PROCEDURES

Surgery, physiology, perfusion, and histology

All procedures were approved by the Institutional Animal Care and Use Committees of the University of California at Berkeley and the University of California at San Francisco, and followed guidelines of the National Institutes of Health (‘Principles of Laboratory Animal Care’, publication no. 85-23). Methods for anesthesia, surgery, physiology, and histology followed those in earlier studies (Lee et al., 2004a; Lee et al., 2004b). Experiments were conducted on seven female and one male adult cats, weighing 2.8–3.5 kg, and free of middle ear disease. Animals were sedated by intramuscular injections of ketamine (22 mg/kg) and acepromazine (0.11 mg/kg), then anesthetized with sodium pentobarbital (15–30 mg/kg; i.v.). Glass pipets (20–30 μm tip diameter) attached to a nanoliter pump (World Precision Instruments, Sarasota, FL) deposited tracers in pulses of 4.6 nl/second. CF responses were mapped in four animals using standard physiological protocols (Lee et al., 2004a) in which single-and multiunit activity in the major thalamic recipient zone, layers IIIb and IV (Winer, 1984a; Winer, 1984c; Winer, 1984b), was recorded with parylene-coated tungsten microelectrodes (0.5–2.5 MΩ). The CF was defined as the frequency at which the lowest sound pressure level stimulus (3 ms linear rise and fall; 50 ms total duration; 400–700 ms interstimulus interval) evoked a response. The CF responses were used to define isofrequency loci within AI and AAF, into which a total of 55.2 nl of CTβ or CTβG (List Biological Laboratories, Campbell, CA) was injected at 500, 1000, and 1500 μm beneath the pia.

In four other, unmapped experiments, tracers were injected into different loci within the same, anatomically identified area. Because tracer spread is <1 mm and a larger injected area might enhance the labeling of BAs, two or three penetrations were made for each tracer (Table 1). To reduce diffusion along the injection track, the pipet remained in place 5 min after the deposit. The unmapped experiments document the global distribution of double labeled neurons outside the primary areas.

Cells labeled with CTβ, CTβG, or both were distinguished readily (Fig. 1C). In two cases (Table 1), WAHG was used instead of CTβG; the ensuing labeling appeared identical. The animals received a lethal dose of sodium pentobarbital 3–4 days after tracer injection and were perfused transcardially with 4% paraformaldehyde/0.1 M phosphate-buffered saline (PBS). Brains were dissected, photographed, and blocked stereotaxically, then cryoprotected for 72 h in 30% sucrose/4% paraformaldehyde/0.1 M PBS.

Transverse frozen sections 60 μm thick were cut in a 1:6 series and processed for the tracers, Nissl staining, or SMI-32 immunostaining; the extra sections were reserved. For CTβG labeling, they were rinsed in 50% ethanol, washed in double distilled water, silver-intensified for 1 h (Kierkegaard and Perry Laboratories, Gaithersburg, MD), washed in 1% sodium thiosulfate, and then in 0.1 M PBS. For CTβ processing, these sections were blocked for 1 h in 5% normal rabbit serum/0.3% Triton X-100, incubated overnight in a 1:7500 dilution of goat anti-CTβ primary antibody (List Biological Laboratories, Campbell, CA) in 0.1 M PBS, and processed using a goat Vectastain avidin-biotin-peroxidase (ABC) kit (Vector Laboratories, Burlingame, CA) with diaminobenzidine (DAB) as the chromogen, then mounted, cleared, and coverslipped.

Adjacent series of sections were prepared with the Nissl stain or immunostained for SMI-32 to delineate thalamic nuclei or cortical areas, respectively. The monoclonal SMI-32 antibody binds to pyramidal cell neurofilaments (Sternberger and Sternberger, 1983) and local patterns of immunoreactivity and Nissl cytoarchitecture were used to identify the thirteen AC areas (Lee and Winer, 2005; Mellott et al., 2005). For the SMI-32 procedure, non-specific immunostaining was blocked by 1 h incubation in 5% normal horse serum/0.3% Triton X-100, and the tissue was incubated overnight in a 1:2000 solution of SMI-32 antibody (Sternberger Monoclonal Inc., Baltimore, MD), and processed with a mouse Vectastain ABC kit (Vector Laboratories) using a heavy-metal intensified DAB chromogen (Adams, 1981). Sections were mounted, cleared and coverslipped.

Anatomical analysis

Labeled neuronal cell bodies were plotted at 20x using a microscope connected to a motorized stage and the Neurolucida interface system (MicroBrightField, Colchester, VT), and from the superficial 20 μm of each section. This ensured that the differential penetration of antibodies for CTβ visualization and silvering agents for CTβG visualization did not lead to an underestimation of double labeling (see Discussion). Thalamic subdivisions were drawn at 15x from Nissl preparations. Sulcal patterns obtained from photographs were used with 15x drawings of SMI-32 stained sections to reconstruct scaled, lateral views of the hemispheres. Areal subdivisions were established using the SMI-32 in conjunction with the Nissl preparations. Neuroexplorer software (MicroBrightField) was used to create three-dimensional cortical reconstructions onto which plots of labeled cells from transverse sections were superimposed. Plots were aligned with scanned Nissl drawings or lateral view schematics using Canvas graphics software (Deneba Software Inc., Miami, FL).

An overlap zone was defined as a series of sections with cells labeled by both tracers; a one section gap arising from technical problems (e.g., antibody penetration) was not considered to interrupt the series. An overlap zone was not defined for structures spanning less than three

contiguous sections. Percentages of double labeled neurons (PDLs) were then calculated both for a nucleus or area and for the overlap zone within it.

Rostrocaudal distributions were constructed for all structures spanning more than three sections. The caudorostral length of a structure was normalized, with the first section containing labeled cells defined as "0," the last as "100". The labeling percentage in a section was calculated as: (number of cells labeled by tracer × in that section) / (number of cells labeled by a tracer in the structure) * 100.

Cumulative distributions were made from the rostrocaudal distributions. For these distributions, the number reported for the *n*th section in a structure was Σ (percent of labeling/tracer from section 0 to section *n*). Thus, if 3/30 double labeled MGB cells were in the first section, this percentage would be 10% for n=1, and if 3 were in the second section, the value would be 20% (6/30) for n=2.

Statistical analysis

Statistical analyses were performed only for experiments which involved physiologically guided deposits. Because there was no a priori reason to consider frequency as a confounding factor, the four experiments were treated as replications, thus giving an n=4. First, we used an ANOVA to screen for differences between PDLs within (i) nuclei or areas, (ii) the entirety of a structure and the overlap zone, (iii) majority, minority, and overall populations, and (iv) cortical hemispheres. If a difference was detected, a paired *t*-test was used to identify its origin (s). Appropriate software (SPSS Inc., Chicago, Illinois) was used for all statistical analyses.

RESULTS

The CTβ and CTβG/WAHG deposit sites did not overlap (Fig. 1B), even at their perimeters, where only diffusion was present and likely contributed little to the patterns of MGB and AC retrograde labeling. Only deposit sites satisfying this independence criterion (Fig. 1A: circles) were accepted for analysis. A further control (not illustrated) was the many cases available in which deposits in separate areas resulted in PDLs similar to those reported here.

In a representative experiment (Fig. 2) deposits of CTβ and CTβG were made ~1.7 mm apart in temporal cortex (Fig. 1A:7, 2D:Te). The ensuing retrograde labeling in the MGB (Fig. 2A–C: blue and red dots) was concentrated in the dorsal division, especially in its more caudal parts such as the dorsal caudal nucleus (Fig. 2A:DCa), in the lateral part of the suprageniculate nucleus (not shown), and in its medial limb more rostrally (Fig. 2C:Sm). These multisensory affiliations would be predicted based on the proximity of the deposits to the rostral bank of the posterior ectosylvian gyrus, a region with strong extrastriate visual associations (Bowman and Olson, 1988). The MGB DLs (Fig. 2A–C, open circles) were interdigitated among the single labeled CTβ or CTβG neurons.

In the ipsilateral hemisphere, retrogradely labeled cells were abundant along the entire ventral AC convexity from the inferior part of the posterior ectosylvian gyrus to the insular cortex and beyond (Fig. 2D:In). Intermixed CTβ and CTβG labeled cells (Fig. 2D: blue and red dots) extended from the perirhinal cortex inferiorly to the caudal border of the dorsal auditory zone (Fig. 2D:DZ). The heaviest labeling was intrinsic and in area Te, where 1.3% of cells were DLs (Fig. 2D: open circles). The ipsilateral corticocortical labeling was concentrated almost entirely in the non-primary AC, with only the tonotopic ventral posterior field having significant numbers of retrogradely labeled neurons, but no DLs (Fig. 2D:VP).

The commissural retrograde labeling largely mirrored the ipsilateral corticocortical pattern, extending even to the labeling in the ventral (Fig. 2E:Ve) and ventral posterior fields, though

on a much reduced scale (Fig. 2E:VP). The vast majority of the single and double labeling was in area Te, and once again the DLs (Fig. 2E: open circles; 1.8%) were intermingled topographically with the single labeled neurons (Fig. 2E: blue and red dots). Not all areas with retrogradely labeled neurons contained DLs, which were conspicuously absent in area AII and in the entire posterior ectosylvian gyrus.

Double labeling

In the mapped cases, more than 99% of DLs were within overlap zones. In the MGBm (case 1568; Table 1), 11/12 DLs (92%) lay within the overlap zone (a derived from the raw data; cf. Fig. 2), as did 8/11 (73%) in contralateral AAF (case 1599). After paired Te injections, 178/179 (>99%) DLs in MGBd were in the overlap zone. In contrast, in MGBm many DLs (15/25; 60%) lay outside the overlap zone after paired area In injections. However, when considering the MGB, ipsi-, and contralateral cortex in all cases, there was no significant difference between the PDLs within the overlap zone and the entire structure (p>0.1, ANOVA).

Medial geniculate body

Following mapped injections, the PDL in each MGB subdivision was calculated. There was a significant difference between PDLs across thalamic nuclei ($p<0.05$, ANOVA), essentially attributable to the significant difference between the MGBv and the RP ($p<0.05$, paired *t*-test); all other pairs of nuclei had statistically indistinguishable PDLs (Fig. 3A; Table 2).

In unmapped cases, up to 7.7% of cells in the intralaminar thalamic nuclei were double labeled. These were classified as “other”, and treated as a fifth category for analytical purposes. PDLs within thalamic nuclei were calculated as above (Fig. 3C; Table 2). Clearly, the PDLs are greater than in the mapped cases; these results could not be statistically compared with each other or with those of the mapped cases, since each involved a different AC area (see Methods).

Auditory cortex

In the ipsi- and contralateral areas AI and AAF (Fig. 3B; Table 2), PDLs were statistically similar across both areas and hemispheres ($p>0.1$, ANOVA). PDLs in the other eleven AC ipsilateral areas were not significantly different (Table 3; $p>0.1$ ANOVA). Similar PDLs were calculated for the injected areas and their commissural counterparts in the unmapped cases (Fig. 3D, Table 2).

Majority and minority projections

In each nucleus or area, one tracer might label more cells (majority population) than were labeled by the other (minority population). DLs are members of both populations. PDLs in both populations were calculated for all structures in mapped cases. In unmapped cases, the targets of both the majority and minority populations are within the same area, so these calculations were not made. These figures were calculated for both the overlap zone and the entire projection; these values were statistically similar (p>0.1, ANOVA), so only those for the entire projection are shown (Fig. 3E,F).

In the MGB, the majority population PDLs did not differ significantly from those of the overall population ($p>0.1$, ANOVA). However, MGB minority population PDLs differed statistically from those of the overall and majority populations ($p<0.05$, ANOVA). Within the minority population, PDLs in MGB nuclei were indistinguishable ($p>0.05$, ANOVA), although in the overall population, the PDL in the RP was significantly lower than that in the MGBv.

The minority population also had a significantly higher PDLs than the overall and majority populations in both ipsi- and contralateral AI and AAF ($p<0.01$, ANOVA), though individual nuclei could not be implicated in creating this ($p>0.05$, paired *t*-test). Further, a statistically

significant difference in PDLS in the minority population ($p<0.05$, ANOVA) could be attributed to the difference between the PDLs in ipsilateral AAF and ipsilateral AI ($p<0.05$, paired *t*-test) (Fig. 3F).

DISCUSSION

Tracer choice

A dual retrograde tract tracing strategy is ideal for revealing neurons with BAs (Hayes and Rustioni, 1979; Kuypers et al., 1980). However, to be equally accurate, the tracers used must be matched for membrane affinity, injection site size, visualization methods, the likelihood for producing damage affecting transport, and tracer-specific differences in transport rate (Schofield et al., 2007). CTβ and CTβG are good candidates because of their biochemical similarity and extremely high membrane affinities. However, they differ in their diffusibility, and thus injection site sizes, as well as visualization sensitivity. CTβG is physically more massive than CTβ due to its conjugated gold particles and thus diffuses less by accessing fewer membrane uptake zones (Llewellyn-Smith et al., 1990). To address this issue we adjusted the injected volume of CTβG so that the sizes of the injection set (which consisted of several single injections; Methods; Table 1) were approximately equal. In every experiment, labeling was equally extensive for both tracers.

Visualization bias is more difficult to address, since the opacity of silver-coated gold particles enhances the detection of gold-labeled cells relative to CTβ-labeled ones, whose diffuse brown color from the diaminobenzidine reaction precipitate can contrast poorly with the background and could lead to underestimates of both CTβ-labeled neurons and DLs. Further, the antibodies for visualizing CTβ molecules are themselves large macromolecules, which may not penetrate the fixed section entirely, while the silvering reagents for visualizing CTβG are much less restricted by size. We addressed this concern by defining labeled neurons conservatively (Fig. 1B) and by confining the analysis to the superficial 20 μm of the section. Thus, our results may underestimate axonal branching but are internally consistent for each case.

Branched axons and spectral maps

AC areas receive afferent input from the MGB, ispi-, and contralateral AC (Fig. 4). While the present results, and those of previous studies (Fig. 4A–D), confirm the presence of TC BAs, they suggest that such BAs targeting AI and AAF may not be sufficiently numerous to create the spectral maps in them. Comparably low PDLs following frequency-matched deposits in either field have been noted (Fig. 4D) (Morel and Imig, 1987;Lee et al., 2004a). If TC BAs were important in establishing the AC CF maps, then BAs should be numerous and concentrated in MGBv and RP, the tonotopically organized MGB nuclei. However, the highest PDL (2.8%) was in the RP, with the only significant difference in nuclear PDLs between the RP and the MGBv, the latter having the lowest value (Fig. 3A;Table 2). Even fewer BAs in both the corticocortical and commissural systems (Fig. 3B;Table 2) suggest that they do not create multiple tonotopic AC maps unless their axons were to ramify far more extensively than is presumed to be the case (Code and Winer, 1986).

Our PDLs in the MGBv are lower than those in a prior study (Morel and Imig, 1987), which may have used more comparable tracers; however, the prior study pooled counts in six sections from five experimental animals, whereas we included every section with labeling in a structure to capture the full TC, corticocortical, and commissural projections. Qualitatively, however, both findings are in accord.

We assayed only one potential variable, CF, that might use BAs as a substrate. There is a substantial representation of binaural response class in both the MGBv and AI (Middlebrooks

and Zook, 1983; Middlebrooks et al., 1989; Brandner and Redies, 1990), and, if a similar representation was accessible elsewhere in AC, we might match injection sites on the basis of binaural responses (Fig. 4C). However, the small apparent size of the binaural response bands might make it difficult to double label sufficient neurons to assess the contribution of BAs, since deposits large enough to produce double labeling may be too large to remain within the rather small and variable aural modules. Moreover, it is unclear how the contribution from other included representations (amplitopy, bandwidth, threshold, etc.) that each covary in AI, could be excluded (Ehret, 1997; Schreiner and Winer, 2007). Although our results suggest that BAs do not create AI and AAF spectral maps, they are limited to this pair of areas. Since AI and AAF are at the same hierarchical level and the posterior auditory field (P) is at a higher one (Rouiller et al., 1991; Lee and Winer, 2005), perhaps more BAs link AI and AAF. Surprisingly, it was reported that the PDLs following frequency matched injections in AI and AAF were similar to those following matched injections in AI and P, suggesting a general paucity of TC BAs in spectral map creation (Morel and Imig, 1987).

Majority and minority populations

Despite the sparse axonal collateralization, the minority PDL population is significantly higher in all structures (Fig. 3E,F). Nearly 20% of RP TC afferents to AI project to AAF as well, and cortical values can reach 12% (contralateral AAF). These results suggest that specific contributions can arise from BAs, though their function, and the rules governing their organization are unknown.

Our values for minority projections are lower than prior ones (Morel and Imig, 1987), which find 56% double-labeling within the minority projection from MGBv-to-AAF (compared to an average of 2.3% in our study) and 35% in the RP-to-AI projection (16.1% in our study). Again, however, their sampling regime differs from ours and may not represent all such branched projections. Nonetheless, as discussed below, more minority population branching may be a general feature of forebrain sensory axons.

Intraareal axonal branching

Intraareal BAs are also sparse, and with no obvious distinction based on the functional class of the target area. However, the PDLs in the thalamus and cortex (Fig. 3E,F; Table 2) are higher than those in the mapped injections. Thus, intraareal branching may be more extensive than the physiologically guided, interareal form. In the TC projection system, intraareal branching may be far greater in non-primary areas. Unfortunately, because each area was only injected in one experimental animal, we cannot make claims of statistical significance from the quantitative data.

Injection site separation may affect PDLs. If a point-to-point connectivity model proposed for AI (Brandner and Redies, 1990) extended throughout AC, double labeling would vary inversely with the distance between injection sites, as confirmed in cat area 17 (Salin et al., 1989). We cannot definitively confirm this principle in AC because different areas were injected in each experiment. However, anterograde studies in cat AC show area specific, differential arborization patterns of TC afferents (Huang and Winer, 2000). It is plausible that an inverse relationship between injection site separation and thalamic PDLs (at least) will hold for all AC areas analyzed here, though it will reflect area-dependent differences in arborization. Finally, intraareal branching may occur on a finer, intralaminar scale, which we did not examine (Fig. 4E).

Axonal branching in other modalities

Many studies of BAs using dual retrograde tract tracing techniques are available for the auditory and visual forebrain. However, because they used various sampling regimes and tracers, direct comparisons can be made only in a few cases.

DLs concentrate largely within overlap zones. In the somatic sensory thalamus, the thalamic cells labeled by unmapped SI and SII injections form concentric rings: the core, in the ventroposterior medial nucleus (VPM) contains only a projection to the primary somatosensory cortex (SI); an inner shell projects to areas SI and SII, and has branched projections to both; and an outer shell region has the same types of labeling but with a coarser topography (Spreafico et al., 1981). The latter authors suggested that secondary, ostensibly less topographic areas arose earlier in evolution (Diamond and Hall, 1969), and that BAs may contribute to the emergence of precise, topographic connections. However, such circumscribed regions of labeling are not readily apparent in the MGB, perhaps because AI and AAF are at the same hierarchical level of processing (Rouiller et al., 1991), because all AC extrinsic connections are topographic (Lee and Winer, 2005), or because the tracers we used may be more sensitive. Second, minority populations have higher PDLs in both the auditory and visual forebrain. For instance, BAs are more common in the A-lamina of the lateral geniculate nucleus (LGN) projection to area 18 than that to area 17 (Bullier et al., 1984a; Birnbacher and Albus, 1987).

Interareal, physiologically guided BAs may be more numerous in the visual forebrain than in the somatic sensory or auditory forebrains. Following mapped injection into matched Pacinian corpuscle response foci in both areas SI and SII, 1.7–2.3% of labeled VPM cells had BAs (Fisher et al., 1983). This value closely approximates those seen in the present study. On the other hand, unmapped deposits in SI/SII yielded PDLs ranging from 14–20% in one cat ventroposterior lateral nucleus (Spreafico et al., 1981), again with an unknown sampling regime.

Reports of the magnitude of visual TC BAs vary as well, from 16% of LGN A-lamina neurons projecting to retinotopically-matched loci in area 17 and 18, to even higher figures in the visual association nuclei (32% in the medial intralaminar nucleus) (Bullier, 1984). Another study found only 3% of LGN A–lamina cells double labeled after retinotopically matched deposits in areas 17 and 18, with lower PDLs in other subcortical structures, e.g. 14% in the medial intralaminar nucleus (Birnbacher and Albus, 1987). They ascribe the difference to their injection sites, which focused on visual field representations 20–40° from the midline, and suggest that the injection sites from Bullier et al. (1984a) may have crossed the area 17–18 boundary. While this may resolve the differences between these studies, it cannot explain the difference between our results and those of others (Bullier, 1984; Birnbacher and Albus, 1987). Our deposits span frequency values across AI and AAF, with injections ranging from 2.1 mm (case 1568) to 7.8 mm apart (case 1572). However, there was no substantial difference in PDLs between these cases despite their marked injection site separation difference. Visual ipsilateral corticocortical connections may have more extensive BAs than auditory ones, with some caveats. In the visual forebrain, corticocortical PDLs following retinotopically matched deposits in areas 17 and 18 are higher in hierarchically advanced areas (for example, 9.5% in area 19 and 20% in area 20) with primarily feedback connections (Bullier et al., 1984b). However, the modest PDLs after retinotopically-matched area 17 and 19 injections (2.5% in area 18 and 4% in area 20) suggests that higher level feedback to other areas uses BAs more strongly if the these areas are at the same hierarchical level. This is not true in AC: branching is distributed across many ipsilateral AC areas, and while some areas had higher PDLs than either AI or AAF, these differences were not significant.

Finally, intraareal BAs are more common in the visual than in the auditory forebrain, but less so than the interareal type noted above. Our paired AI injections (3.3 mm apart) are comparable

to injections into area 17 (3.4 mm apart), and the corresponding PDLs in the MGBv/LGN lamina A, respectively, are both less than 1.5% (Salin et al., 1989). However, BAs are somewhat more common in other cortical areas converging on area 17 (3–7%) than in the corticocortical pathways converging on AI (0.8–2.1%).

It is not surprising that BAs follow different rules in the visual, somatic sensory, and auditory systems, as there may be submodality-specific differences. For example, LGN X-cell axons do not branch to areas 17 and 18, while 17% of LGN A-lamina cells target both areas-a value that rises to 50% in the LGN C lamina (Humphrey et al., 1985). Thus, there are modality-specific, and perhaps submodality-specific, BA organizing principles.

Auditory system branched axons

Physiologically guided, interareal TC BAs may not create the CF maps in AI and AAF (or, by extension, the other three AC maps), and intraareal branching is sparse. However, both types of branched projection have an organization that differs from their unbranched counterparts. Thus, BAs are ubiquitous in the auditory forebrain connectional systems, though sparse numerically (Fig. 4E–G).

These results can be reconciled with the results of anterograde studies reporting extensive arborization (Huang and Winer, 2000) (Fig. 4E) by considering that a deposit will label collaterals based on injection site separation and the relative orientations of, and alignment between, the collaterals and the deposit across the cortex.

Our results support the view that the auditory forebrain BA organization differs from that of the subcortical auditory system, where axon collateralization can be extensive (Irvine, 1986). Intracellular filling studies report over 50% collateralization of axons, both intra- and interareally, from the medial and lateral nuclei of the trapezoid body to the medial and lateral superior olives in the mustache bat, big brown bat, mouse, and gerbil (Kuwabara and Zook, 1992). Most guinea pig dorsal cochlear nucleus neurons were double labeled after bilateral injections of the inferior colliculus (IC) (Schofield and Cant, 1996). Bilateral injections of retrograde tracers in the guinea pig cochlear nuclei yielded extensive periolivary double labeling, especially the ventral periolivary nuclei (Schofield and Cant, 1999).

However, BAs are not extensive in all subcortical auditory projections. For example, bilateral injections of guinea pig CN resulted in <1% double labeling in the IC (Schofield, 2001). Further, in the rat, <1% of IC neurons were double labeled after injections into various combinations of the MGB, contralateral IC, CN, or superior olivary complex (Okoyama et al., 2006). Corticofugal projections likewise appear to have few BAs, with no AI neurons projecting to both the ipsilateral MGB and contralateral AI, or to ipsilateral MGB and IC (Wong and Kelly, 1981).

The function of these forebrain BAs remains unclear. Given the precision of developing connections and the efficient ontogenetic elimination of transient axon collaterals (Innocenti and Clarke, 1984; Clarke and Innocenti, 1986; Kadhim et al., 1993), BAs would seem unlikely candidates to be remnants of developmental error. Because BAs are present in all three projection systems that construct the spectral maps in AI and AAF, they might be part of the widespread, functionally masked, latent anatomical substrate for spectral map reorganization (Jacobs and Donoghue, 1991). However, BAs are clearly sparser than heterotopic projections, which may also be involved in AC plasticity (Fig. 4F–H) (Lee et al., 2004b). To understand the function of these branched projections, their microanatomical organization and the electrophysiological properties of their synaptic connections must be determined.

Acknowledgments

We honor Professor Kristin Kjelsberg Osen for her many contributions to experimental neuroanatomy. We thank Drs. C.E. Schreiner and K. Imaizumi for generously sharing experimental data from the mapped experiments. Supported by NINCDS grant R01 DC02319-29.

REFERENCES

Adams JC. Heavy metal intensification of DAB-based HRP reaction product. J Histochem Cytochem 1981;29:775. [PubMed: 7252134]

Aitkin LM, Webster WR. Medial geniculate body of the cat: organization and responses to tonal stimuli of neurons in ventral division. J Neurophysiol 1972;35:365–380. [PubMed: 5029955]

Basbaum AI, Menetrey D. Wheat germ agglutinin-apoHRP gold: a new retrograde tracer for light- and electron-microscopic single- and double-label studies. J Comp Neurol 1987;261:306–318. [PubMed: 2442205]

Birnbacher D, Albus K. Divergence of single axons in afferent projections to the cat's visual cortical areas 17, 18, and 19: a parametric study. J Comp Neurol 1987;261:543–561. [PubMed: 2440917]

Bowman EM, Olson CR. Visual and auditory association areas of the cat's posterior ectosylvian gyrus: cortical afferents. J Comp Neurol 1988;272:30–42. [PubMed: 2454976]

Brandner S, Redies H. The projection of the medial geniculate body to field AI: organization in the isofrequency dimension. J Neurosci 1990;10:50–61. [PubMed: 1688936]

Bullier, J. Axonal bifurcation in the afferents to cortical areas of the visual system. In: Pettigrew, JD., et al., editors. Visual Neuroscience. London: Cambridge University Press; 1984. p. 239-259.

Bullier J, Kennedy H, Salinger W. Bifurcation of subcortical afferents to visual areas 17, 18, and 19 in the cat cortex. J Comp Neurol 1984a;228:308–328.

Bullier J, Kennedy H, Salinger W. Branching and laminar origin of projections between visual cortical areas in the cat. J Comp Neurol 1984b;228:329–341. [PubMed: 6434600]

Clarke S, Innocenti GM. Organization of immature interhemispheric connections. J Comp Neurol 1986;251:1–22. [PubMed: 3760253]

Code RA, Winer JA. Columnar organization and reciprocity of commissural connections in cat primary auditory cortex (AI). Hearing Res 1986;23:205–222.

Diamond IT, Hall WC. Evolution of neocortex. Science 1969;164:251–262. [PubMed: 4887561]

Ehret G. The auditory cortex. J Comp Physiol A 1997;181:547–557. [PubMed: 9449816]

Fisher GR, Freeman B, Rowe MJ. Organization of parallel projections from Pacinian afferent fibers to somatosensory cortical areas I and II in the cat. J Neurophysiol 1983;49:75–97. [PubMed: 6827305]

Hayes NL, Rustioni A. Dual projections of single neurons are visualized simultaneously: use of enzymatically active ^{3}H-HRP. Brain Res 1979;165:321–326. [PubMed: 84698]

Huang CL, Winer JA. Auditory thalamocortical projections in the cat: laminar and areal patterns of input. J Comp Neurol 2000;427:302–331. [PubMed: 11054695]

Humphrey AL, Sur M, Uhlrich DJ, Sherman SM. Termination patterns of individual X- and Y-cell axons in the visual cortex of the cat: projections to area 18, to the 17/18 border region, and to both areas 17 and 18. J Comp Neurol 1985;233:190–212. [PubMed: 3973101]

Imig TJ, Morel A. Tonotopic organization in ventral nucleus of medial geniculate body in the cat. J Neurophysiol 1985;53:309–340. [PubMed: 3973661]

Innocenti GM, Clarke S. Bilateral transitory projections to visual areas from auditory cortex in kittens. Dev Brain Res 1984;14:143–148.

Irvine, DRF. The Auditory Brainstem. A Review of the Structure and Function of Auditory Brainstem Processing Mechanisms. In: Autrum, H., et al., editors. Progress in Sensory Physiology. vol. 7. 1986. p. 1-279.

Jacobs KM, Donoghue JP. Reshaping the cortical motor map by unmasking latent intracortical connections. Science 1991;251:944–947. [PubMed: 2000496]

Kadhim HJ, Bhide PG, Frost DO. Transient axonal branching in the developing corpus callosum. Cereb Cort 1993;3:551–566.

Kawamura K. Corticocortical fiber connections of the cat cerebrum. I. The temporal region. Brain Res 1973;51:1–21. [PubMed: 4706011]

Kuwabara N, Zook JM. Projections to the medial superior olive from the medial and lateral nuclei of the trapezoid body in rodents and bats. J Comp Neurol 1992;324:522–538. [PubMed: 1430335]

Kuypers HGJM, Bentivoglio M, Catsman-Berrevoets CE, Bharos AT. Double retrograde labeling through divergent axons collaterals, using two fluorescent tracers with the same excitation wavelength which label different features of the cell. Exp Brain Res 1980;40:383–392. [PubMed: 6160043]

Lee CC, Imaizumi K, Schreiner CE, Winer JA. Concurrent tonotopic processing streams in auditory cortex. Cereb Cort 2004a;14:441–451.

Lee CC, Schreiner CE, Imaizumi K, Winer JA. Tonotopic and heterotopic projection systems in physiologically defined auditory cortex. Neuroscience 2004b;128:871–887. [PubMed: 15464293]

Lee CC, Winer JA. Principles governing auditory forebrain connections. Cereb Cort 2005;15:1804–1814.

Llewellyn-Smith IJ, Minson JB, Wright AP, Hodgson AJ. Cholera toxin B-gold, a retrograde tracer that can be used in light and electron microscopic immunocytochemical studies. J Comp Neurol 1990;294:179–191. [PubMed: 1692043]

Luppi P-H, Fort P, Jouvet M. Iontophoretic application of unconjugated cholera toxin B subunit (CTb) combined with immunohistochemistry of neurochemical substances: a method for transmitter identification of retrogradely labeled neurons. Brain Res 1990;534:209–224. [PubMed: 1705851]

MacKenzie CR, Hirama T, Lee KK, Altman E, Young NM. Quantitative analysis of bacterial toxin affinity and specificity for glycolipid receptors by surface plasmon resonance. J Biol Chem 1997;272:5533–5538. [PubMed: 9038159]

Mellott JG, Van der Gucht E, Lee CC, Larue DT, Winer JA, Lomber SG. Subdividing cat primary and non-primary auditory areas in the cerebrum with neurofilament proteins expressing SMI-32. Assn Res Otolaryngol 2005;28:994.

Middlebrooks JC, Makous JC, Green DM. Directional sensitivity of sound-pressure levels in the human ear canal. J Acoust Soc Am 1989;86:89–108. [PubMed: 2754111]

Middlebrooks JC, Zook JM. Intrinsic organization of the cat's medial geniculate body identified by projections to binaural response-specific bands in the primary auditory cortex. J Neurosci 1983;3:203–225. [PubMed: 6185655]

Morel A, Imig TJ. Thalamic projections to fields A, AI, P, and VP in the cat auditory cortex. J Comp Neurol 1987;265:119–144. [PubMed: 2826552]

Morel A, Rouiller E, de Ribaupierre Y, de Ribaupierre F. Tonotopic organization in the medial geniculate body (MGB) of lightly anesthetized cats. Exp Brain Res 1987;69:24–42. [PubMed: 3436391]

Okoyama S, M O, Ito M, Harada S. Neuronal organization of the rat inferior colliculus participating in four major auditory pathways. Hearing Res 2006;218:72–80.

Rose, JE.; Woolsey, CN. Cortical connections and functional organization of thalamic auditory system of cat. In: Harlow, HF.; Woolsey, CN., editors. Biological and Biochemical Bases of Behavior. Madison: University of Wisconsin Press; 1958. p. 127-150.

Rouiller EM, Simm GM, Villa AEP, de Ribaupierre Y, de Ribaupierre F. Auditory corticocortical interconnections in the cat: evidence for parallel and hierarchical arrangement of the auditory cortical areas. Exp Brain Res 1991;86:483–505. [PubMed: 1722171]

Salin PA, Bullier J, Kennedy H. Convergence and divergence in the afferent projections to cat area 17. J Comp Neurol 1989;283:486–512. [PubMed: 2745751]

Schofield BR. Origins of projections from the inferior colliculus to the cochlear nucleus in guinea pigs. J Comp Neurol 2001;429:206–220. [PubMed: 11116215]

Schofield BR, Cant NB. Origins and targets of commissural connections between cochlear nuclei in guinea pigs. J Comp Neurol 1996;375:128–146. [PubMed: 8913897]

Schofield BR, Cant NB. Descending auditory pathways: projections from the inferior colliculus contact superior olivary cells that project bilaterally to the cochlear nuclei. J Comp Neurol 1999;409:210–223. [PubMed: 10379915]

Schofield BR, Schofield RM, Sorensen KA, Motts SD. On the use of retrograde tracers for identification of axon collaterals with multiple fluorescent retrograde tracers. Neuroscience 2007;146:773–783. [PubMed: 17379419]

Schreiner CE, Winer JA. Auditory cortex mapmaking: principles, projections, and plasticity. Neuron 2007;56:356–365. [PubMed: 17964251]

Spreafico R, Hayes NL, Rustioni A. Thalamic projection on the primary and secondary somatosensory cortices in cat: single and double retrograde tracer studies. J Comp Neurol 1981;203:67–90. [PubMed: 6273459]

Sternberger LA, Sternberger NH. Monoclonal antibodies distinguish phosphorylated and nonphosphorylated forms of neurofilaments in situ. Proc Natl Acad Sci USA 1983;80:6126–6130. [PubMed: 6577472]

Winer JA. Anatomy of layer IV in cat primary auditory cortex (AI). J Comp Neurol 1984a;224:535–567. [PubMed: 6725630]

Winer JA. The non-pyramidal neurons in layer III of cat primary auditory cortex (AI). J Comp Neurol 1984b;229:512–530. [PubMed: 6501610]

Winer JA. The pyramidal cells in layer III of cat primary auditory cortex (AI). J Comp Neurol 1984c; 229:476–496. [PubMed: 6209308]

Winer JA, Lee CC. The distributed auditory cortex. Hearing Res 2007;229:3–13.

Winer JA, Saint Marie RL, Larue DT, Oliver DL. GABAergic feedforward projections from the inferior colliculus to the medial geniculate body. Proc Natl Acad Sci USA 1996;93:8005–8010. [PubMed: 8755593]

Wong D, Kelly JP. Differentially projecting cells in individual layers of the auditory cortex: a double-labeling study. Brain Res 1981;230:362–366. [PubMed: 7317785]

Abbreviations

AAF, anterior auditory field
AES, anterior ectosylvian sulcus
AI, primary auditory cortex
AII, second auditory cortical area
APt, anterior pretectum
BIC, brachium of the inferior colliculus
CG, central gray
CTβ, cholera toxin β subunit
CTβG, cholera toxin β subunit gold conjugate
D, dorsal nucleus of the MGB *or* dorsal
DCa, caudal dorsal nucleus of the MGB
DD, deep dorsal nucleus of the MGB
DS, dorsal superficial nucleus of the MGB dorsal division
DZ, dorsal auditory zone
ED, posterior ectosylvian gyrus, dorsal part
EE, excitatory-excitatory binaural interaction
EI, posterior ectosylvian gyrus, intermediate part *or* excitatory-inhibitory binaural interaction
EV, posterior ectosylvian gyrus, ventral part
In, insular cortex
IIIn, oculomotor nucleus
LGB, lateral geniculate body
LMN, lateral mesencephalic nucleus
M, medial division of the MGB *or* medial
Ov, *pars ovoidea* of the MGB
P, posterior auditory cortical area
PC, posterior commissure
PL, posterior limitans nucleus
Pul, pulvinar
R, rostral
RN, red nucleus

RP, rostral pole division of the MGB
SC, superior colliculus
Sl, supragenicular nucleus, lateral part
Sm, supragenicular nucleus, medial par
Spf, subparafascicular nucleus
SpN, suprapeduncular nucleus
Te, temporal cortical area
V, ventral division of the MGB *or* ventral
Ve, ventral auditory cortical area
Vl, ventrolateral nucleus of the MGB
VP, ventral posterior auditory cortical area

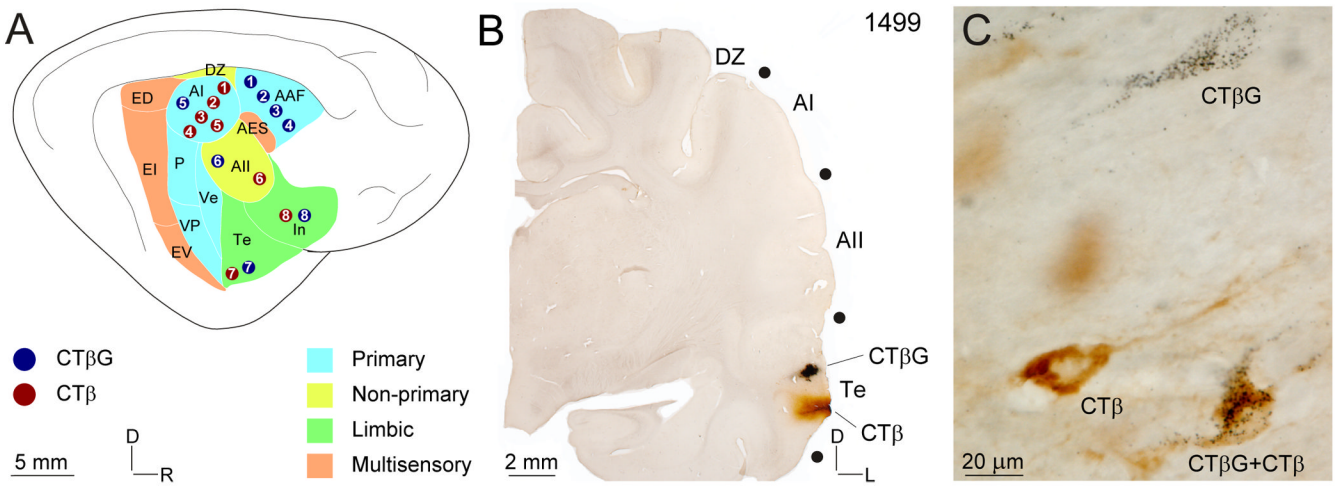

Fig. 1.

Auditory cortex (AC) areas, representative injection sites, and characteristic retrograde labeling. (A) Schematic of AC areas coded by functional class. Circles, deposit sites (blue: CTβG; red: CTβ) ; numbers, experiment. (B) Representative CTβ and CTβG deposit sites in area Te. (C) Types of retrograde labeling: CTβ, CTβG both CTβ and CTβG See Table 1 for a summary of experiments.

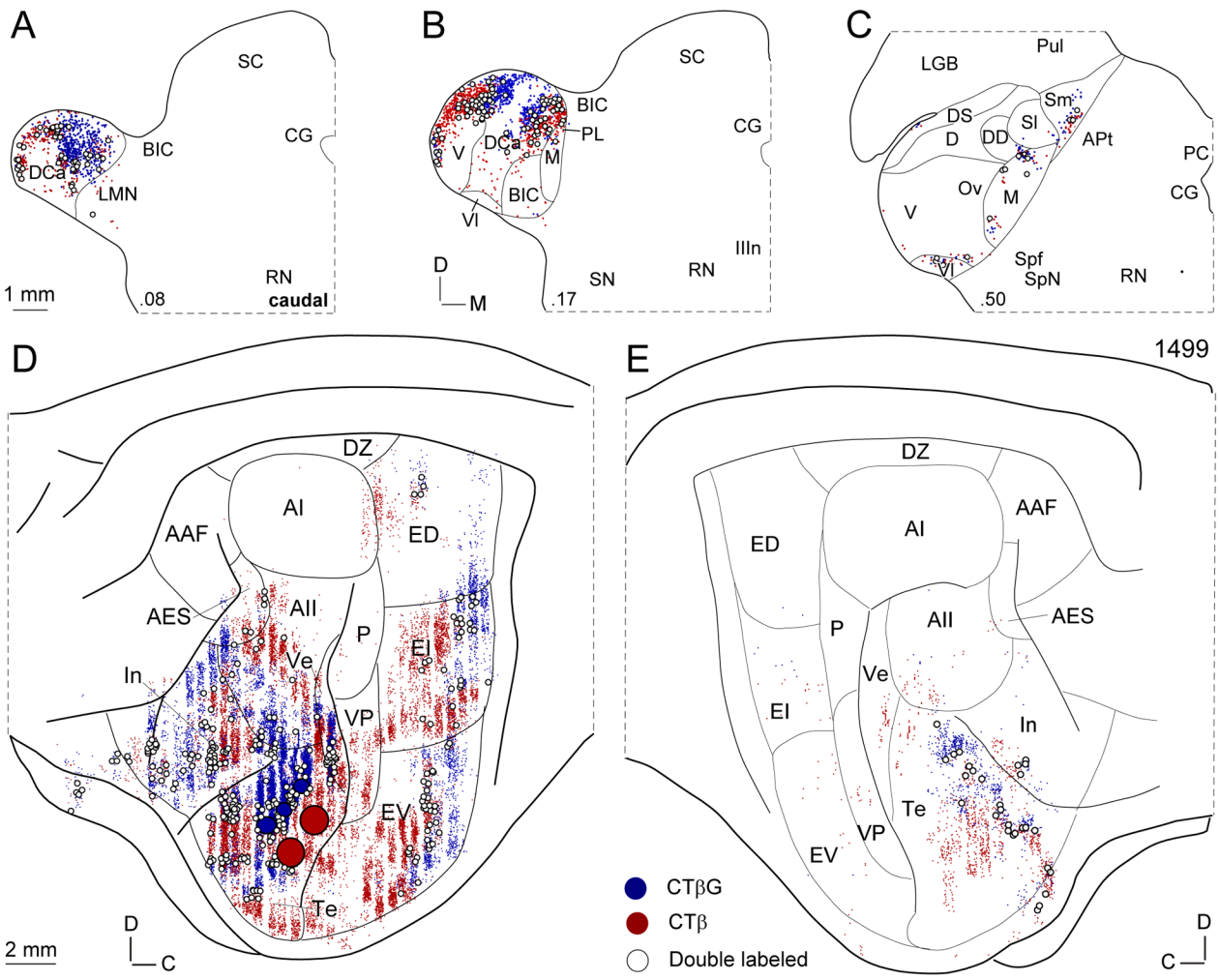

Fig. 2.

Representative retrograde thalamic and cortical labeling. Dots, single labeled cells (blue: CTβG; red: CTβ; open circles, double labeled cells. (A–C) Thalamic labeling after paired injections into area Te. Double labeled neurons (DLs), though relatively sparse are present in all MGB divisions and in the thalamic intralaminar nuclei (not shown for the latter). (D) Ipsilateral corticocortical labeling. DLs are sparse, and distributed more heterogeneously, with most in areas In or Te. Large solid circles, deposit sites (blue: CTβG; red: CTβ). (E) Commissural corticocortical labeling. DLs are rare in this projection system and concentrated in the contralateral, rostral Te.

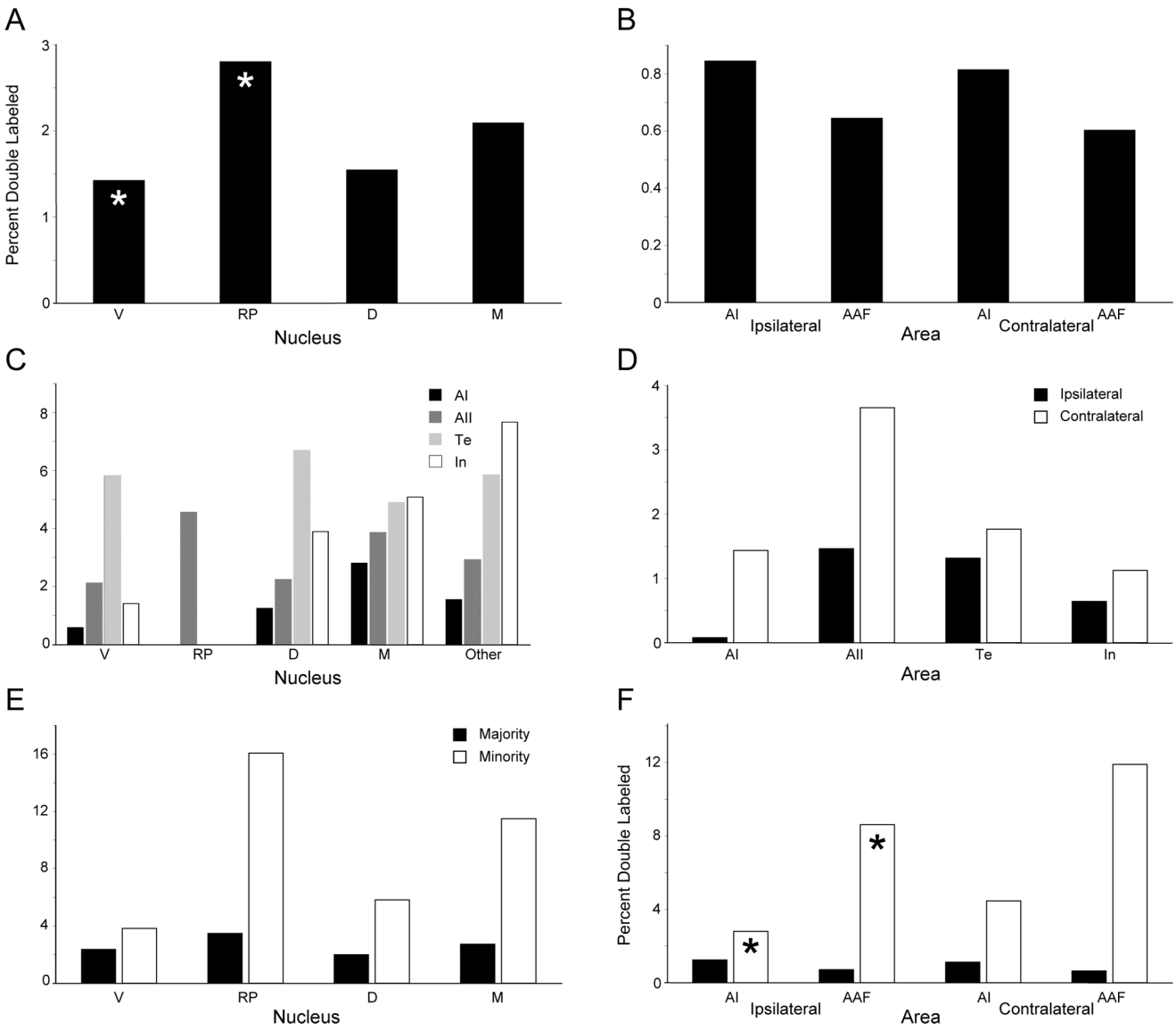

Fig. 3.

Percentages of double labeled neurons (PDLs). (A,B) PDLs in the MGB (A) and AC (B) after frequency-matched deposits of CTβ and CTβG in areas AI and AAF, respectively (Table 2). (C,D) PDLs in the MGB (C) and AC (D) ensuing from unmapped CTβ and CTβG deposits within the same area (Table 2). (E,F) After frequency-matched deposits in AI and AAF, a majority of labeled neurons in a given nucleus or area project to one area and a minority projects to the other. PDLs were calculated in the majority and minority populations of MGB (E) and AC (F) labeled neurons. Asterisks, significant differences ($p<0.05$; paired *t*-test). There is a significant PDLs difference as well between the minority and majority populations in all nuclei and areas ($p<0.05$; see text).

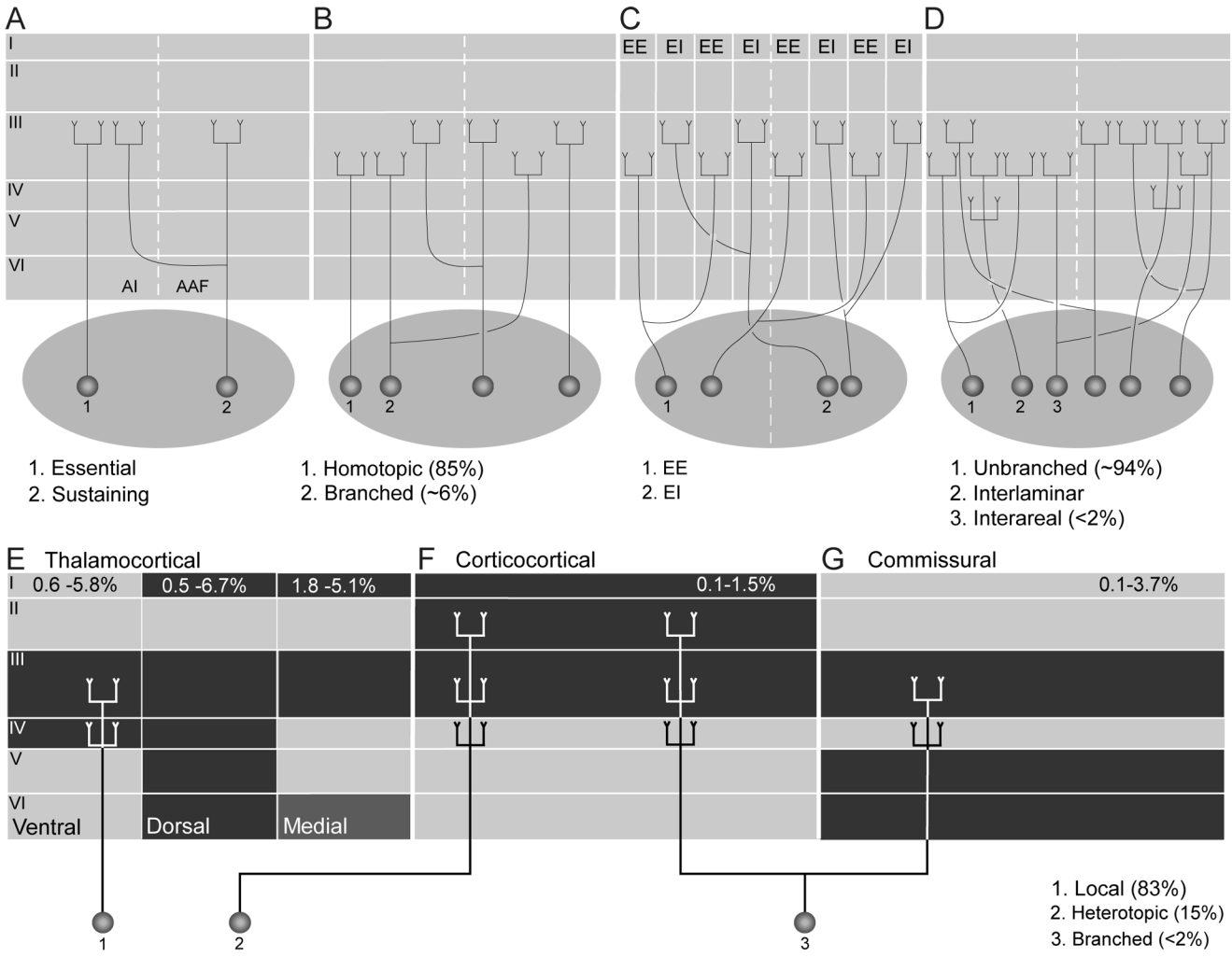

Fig. 4.

(A–D) Models of thalamocortical (TC) axonal branching. Essential and sustaining TC projections suggest that branched and unbranched input reaches AI (Rose and Woolsey, 1958). (B) CF-guided interareal BAs provide a limited (<6%) contribution to the TC projections (Morel et al., 1987). (C) TC BAs may participate in creating binaural bands within areas (Middlebrooks and Zook, 1983) and they are not inconsistent with models of point-to-point TC projections (Brandner and Redies, 1990). (D) Extensive interlaminar and intralaminar TC branching (Huang and Winer, 2000) is superimposed upon sparse interareal branching (Lee et al., 2004a). (E–G) Schematic representations of TC projections integrated with laminar patterns of branched and unbranched models of thalamocortical, corticocortical, and commissural input. (F) Point-to-point, tonotopic projections (1) constitute the majority (85%) of input to AI. Heterotopic projections (F:2), however, represent a substantial (15%) parallel input (Lee et al., 2004b). (F,G) Interareal branching (3) constitutes <2% of the TC input. Black: principal laminar terminations of thalamocortical, corticocortical, and homotypic commissural afferents to AI. TC afferents from (i) type 1 and (ii) type 2 MGB projections terminate principally layers III and IV and (iii) type 3 input reaches layers I and VI as well(Huang and Winer, 2000). (F) Corticocortical afferents to AI (C) end mainly in layers I, III, and IV (Kawamura, 1973). (G) Many homotypic commissural axons target layers III, V, and VI in AI (Code and Winer, 1986).

Table 1

Summary of experiments

Summary of experiments: areas injected, tracers, survivals, and deposit site separation.

Experiment	CTβG[1]	CTβ	Deposit Separation (mm)	Survival (days)
1439	AI (3)[2]	AI (2)	3.3	3
1444	AII (3)[2]	AII (2)	3.3	4
1499	Te (3)	Te (2)	1.7	3
1524	In (2)	In (2)	1.5	4
1572 (3 kHz)	AAF (1)	AI (3)	7.8	3
1561 (7 kHz)	AAF (1)	AI (2)	7.5	3
1599 (20 kHz)	AAF (1)	AI (3)	2.5	3
1568 (30 kHz)	AAF (1)	AI (3)	2.1	3

[1] Number of deposits.

[2] WAHG used instead of CTβG.

Table 2

Thalamic and Cortical Double Labeled Cells

Thalamic and cortical percentages of double labeled cells (PDLs). The PDL in V is significantly lower than in RP ($p<0.05$; paired *t*-test).

	MGB				AC	
Experiment	**V**	**RP**	**D**	**M**	**Ipsilateral**[1]	**Contralater al**
1439 (AI)	1.4[2](21/1492)[3]	0 (0/0)	1.3 (3/240)	0.5 (12/2500)	0.1 (18/25154)	1.7 (10/597)
1444 (AII)	2.1 (15/711)	4.5 (2/44)	2.2 (50/2234)	3.9 (29/752)	1.7 (462/27601)	3.7 (80/2189)
1499 (Te)	5.8 (26/449)	0 (0/0)	6.7 (179/2680)	4.9 (15/307)	1.3 (194/14768)	1.8 (26/1474)
1524 (In)	1.4 (7/497)	0 (0/0)	3.9 (103/2649)	5.1 (25/492)	0.6 (359/55986)	1.1 (15/1334)
1572 (3 kHz)	1.1 (14/1325)	2.1 (9/426)	0.9 (4/451)	1.8 (6/328)	0.5 (72/15713), 0.3 (77/25539)	0.2 (3/1502), 0.2 (5/2159)
1561 (7 kHz)	1.8 (15/857)	2.7 (7/256)	0.5 (1/210)	1.5 (2/137)	0.2 (21/11376), 0.6 (82/13047)	0.1 (1/968), 0.6 (4/732)
1599 (20 kHz)	0.8 (14/1696)	3.3 (15/449)	3.3 (14/423)	2.4 (7/294)	1.3 (152/11940), 0.6 (135/21401)	0.7 (5/768), 0.8 (11/1424)
1568 (30 kHz)	2.0 (33/1610)	3.0 (29/964)	1.3 (3/226)	2.7 (12/446)	1.5 (706/48189), 1.0 (309/30387)	2.3 (38/1635), 0.9 (14/1634)

[1] Cortical area injected (1439, 1522) or AI, AAF (1572, 1599).

[2] Percentages.

[3] Raw numbers.

Table 3

Cortical Labeled Cells (Heterotypic)

Double labeled cortical cells (heterotypic). PDLs in eleven other AC areas after frequency-matched injections in AI and AAF. No significant differences were found ($p>0.05$, paired t-test).

	Experiment				
Area	1572 (3 kHz)	1561 (7 kHz)	1599 (20 kHz)	1568 (30 kHz)	Average
P	0.4[1] (19/4281)[2]	0.9 (10/1151)	0.6 (5/897)	1.6 (34/2088)	0.9
VP	0.7 (13/1839)	0.6 (10/1632)	2.0 (15/740)	4.5 (56/1247)	2.0
Ve	0.9 (6/697)	0.3 (4/1493)	0.4 (3/683)	1.8 (52/2964)	0.8
AII	0.6 (9/1547)	0 (0/362)	1.7 (10/592)	1.7 (20/1160)	1
DZ	0.4 (4/939)	0 (0/1290)	1.6 (10/630)	2.3 (24/1042)	1.1
AES	0 (0/0)	0.8 (2/242)	-	0.6 (3/528)	0.5
Te	1.0 (4/410)	0 (0/62)	0 (0/44)	1.7 (9/520)	0.7
In	3.7 (1/27)	-	-	0 (0/58)	1.9
ED	0 (0/0)	0 (0/77)	-	2.4 (18/795)	0.8
EI	1 (10/979)	1 (6/611)	2.2 (10/456)	4.3 (48/1106)	2.1
EV	1.7 (9/522)	0.5 (1/201)	0.7 (3/405)	2.8 (43/1556)	1.4

[1] Percentages.

[2] Raw numbers.

-, no labeled cells.